Pure and Applied Mathematics Journal
2026, Vol. 15, No. 3, pp. 35–44
https://doi.org/10.11648/j.pamj.20261503.11

SciencePG
Science Publishing Group

Research Article

Mathematical Modeling of Integrated Wind, Thermal, and Tectonic Stress Analysis on Cantilever Balconies Using Ordinary Differential Equations

Titus Leonard Oketch[1, *], **Beatrice Adhiambo Odero Obiero**[1], **Albert Bii**[2]

[1]Department of Mathematics Statistics and Computing, Rongo University, Rongo, Kenya
[2]Department of mathematics and Computer Science, University of Eldoret, Eldoret, Kenya

Abstract

Cantilever balconies are widely used in modern buildings due to their architectural flexibility and efficient use of space. However, their structural performance is highly sensitive to environmental loading because their bending resistance is concentrated at the fixed support. In real service conditions, these structures are simultaneously subjected to static loads, wind-induced aerodynamic forces, seasonal thermal effects, and seismic ground acceleration. Most conventional analyses treat these effects independently, which may underestimate cumulative deflection and lead to inaccurate serviceability predictions. This study develops a unified mathematical model to quantify the total tip deflection of a cantilever balcony subjected to combined static, wind, thermal, and seismic loading. The formulation is based on Euler–Bernoulli beam theory and linear elasticity assumptions. Closed-form analytical expressions are derived for each loading component and integrated using the principle of superposition to obtain a compact total deflection equation. Numerical simulations are performed for aluminum, steel, reinforced concrete, and carbon fiber composites under representative environmental conditions. Results show that thermal effects become dominant in high-temperature environments for materials with large coefficients of thermal expansion, while seismic effects become significant in regions with high peak ground acceleration. Among the materials considered, carbon fiber composites consistently exhibit the smallest total deflection due to their high stiffness and low thermal sensitivity, while reinforced concrete shows the largest deformation due to its lower elastic modulus. The proposed model provides a mathematically consistent framework for evaluating cantilever balcony performance under multi-hazard environmental loading and offers a useful decision-support tool for preliminary structural design and material selection.

Keywords

Cantilever Balcony, Euler–Bernoulli Beam, Wind Loading, Thermal Expansion, Peak Ground Acceleration, Multi-hazard Modeling

1. Introduction

Cantilever balconies are widely used in modern structural systems because they increase usable space without requiring additional vertical support. Their structural behavior, however, differs significantly from simply supported systems because

*Correspondence: Titus Leonard Oketch (woramasleo@gmail.com)

Received: 4 April 2026; **Accepted:** 25 April 2026; **Published:** 11 May 2026

all bending resistance is concentrated at the fixed connection, making them highly sensitive to environmental and mechanical loading effects. Classical structural analysis shows that cantilever deflection scales with the cube of the span length and inversely with flexural rigidity, making stiffness a primary control parameter in serviceability performance [4, 11]. Previous studies have examined individual loading mechanisms affecting cantilever structures. Wind-induced structural response has been extensively studied using both experimental and computational approaches, showing that aerodynamic forces may significantly influence deflection behavior of protruding structural elements [5, 10, 14]. Similarly, thermo-mechanical studies demonstrate that temperature gradients can induce curvature and additional deformation in restrained structural members [2, 9]. Seismic response has also been analyzed within the framework of structural dynamics, where ground acceleration contributes to additional displacement through inertial interaction with structural mass [1, 6, 12]. Despite these advances, most existing studies treat wind, thermal, and seismic effects independently. Recent research suggests that coupled environmental effects may significantly alter structural response when compared to single-hazard approximations [3, 7]. Environmental data used for simulation in this study is obtained from open-source publications [8, 13]. For cantilever balcony systems in particular, limited work exists on unified mathematical formulations that integrate multiple environmental drivers into a single predictive framework. From a mathematical modeling perspective, integrated formulations are desirable because they allow consistent scaling analysis, parameter sensitivity evaluation, and comparative material assessment within a single analytical structure. Such unified models also provide improved preliminary design tools compared to isolated empirical formulations. Motivated by these considerations, this study develops a compact analytical model to quantify the total tip deflection of a cantilever balcony subjected to combined static, wind, thermal, and seismic loading. The formulation is based on Euler–Bernoulli beam theory together with linear elasticity assumptions, and individual deflection contributions are derived analytically and combined using the principle of superposition.

2. Structural Model

2.1. Beam Idealization

The cantilever balcony is modeled as a prismatic Euler–Bernoulli beam of length L, where the longitudinal coordinate $x \in [0, L]$ is measured from the fixed support. The transverse displacement is denoted by $w(x,t)$, where $t$represents time. The beam has constant material and geometric properties: density ρ, cross-sectional area A, Young's modulus E, and second moment of area I. The quantity $EI$is the flexural rigidity, representing the resistance of the beam to bending.

Consider an infinitesimal beam element of length dx. Let $V(x,t)$ denote the internal shear force, $M(x,t)$ the bending moment, and $q(x,t)$the externally applied transverse load per unit length.

Applying Newton's second law in the transverse direction:

$$V(x+dx,t) - V(x,t) + q(x,t)\,dx = \rho A\,dx\,\frac{\partial^2 w}{\partial t^2}$$

where: $V(x+dx,t) - V(x,t)$represents the net change in shear force across the element, $q(x,t)\,dx$is the external distributed load acting on the element, $\rho A\,dx$is the mass of the element and $\frac{\partial^2 w}{\partial t^2}$is the transverse acceleration.

By dividing through by $dx$and taking the limit as $dx \to 0$, we obtain:

$$\frac{\partial V}{\partial x} + q(x,t) = \rho A\frac{\partial^2 w}{\partial t^2}$$

This equation represents dynamic equilibrium between internal shear variation, external loading, and inertia.

From beam theory, the shear force is related to the bending moment by:

$$V = \frac{\partial M}{\partial x}$$

Under the Euler–Bernoulli hypothesis (plane sections remain plane and perpendicular to the neutral axis), the curvature of the beam is approximated by:

$$\kappa \approx \frac{\partial^2 w}{\partial x^2}$$

The bending moment is proportional to curvature:

$$M = -EI\frac{\partial^2 w}{\partial x^2}$$

where: $E$is Young's modulus (material stiffness), $I$is the second moment of area (geometric stiffness) and the negative sign reflects the chosen sign convention for bending.

Differentiate the moment expression:

$$V = \frac{\partial M}{\partial x} = -EI\frac{\partial^3 w}{\partial x^3}$$

Then differentiate again:

$$\frac{\partial V}{\partial x} = -EI\frac{\partial^4 w}{\partial x^4}$$

Substitute into the force equilibrium equation:

$$-EI\frac{\partial^4 w}{\partial x^4} + q(x,t) = \rho A\frac{\partial^2 w}{\partial t^2}$$

Rearranging:

$$\rho A\frac{\partial^2 w}{\partial t^2} + EI\frac{\partial^4 w}{\partial x^4} = q(x,t)$$

Final Governing Equation

$$\rho A \frac{\partial^2 w}{\partial t^2} + EI \frac{\partial^4 w}{\partial x^4} = q(x,t) \quad (1)$$

where ρ is the material density (kg/m^3), A is the cross-sectional area (m^2) so that ρA is the mass per unit length (kg/m), E is Young's modulus (Pa), I is the second moment of area (m^4), and $q(x,t)$ is the distributed load (N/m).

The boundary conditions for a cantilever beam are

$$w(0,t) = 0, \frac{\partial w}{\partial x}(0,t) = 0 \quad (2)$$

$$\frac{\partial^2 w}{\partial x^2}(L,t) = 0, \frac{\partial^3 w}{\partial x^3}(L,t) = 0 \quad (3)$$

representing zero displacement and slope at the fixed end, and zero bending moment and shear force at the free end.

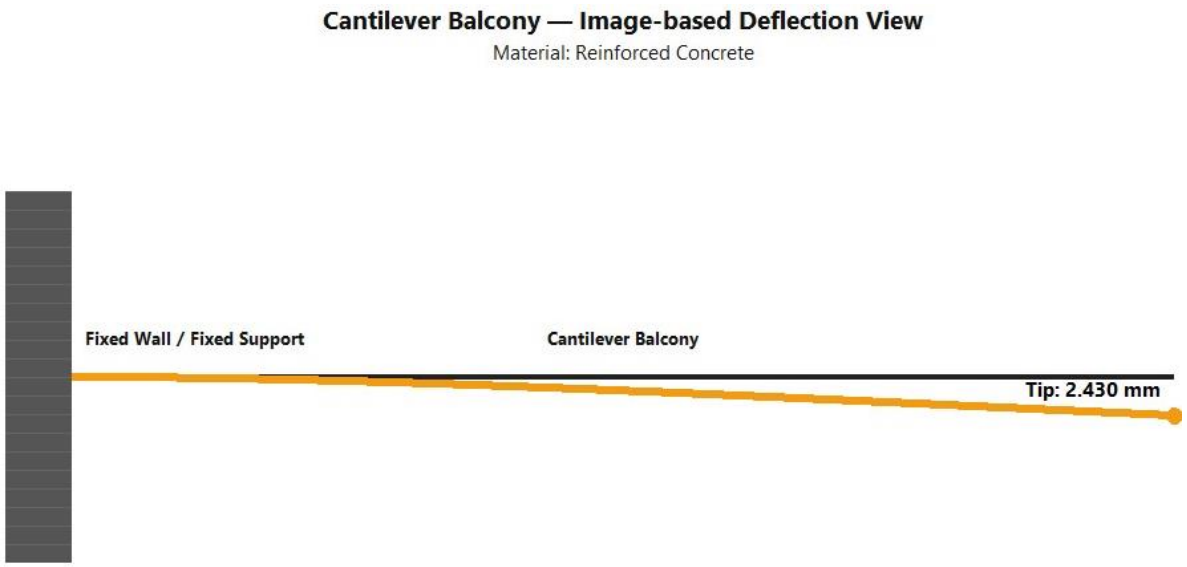

Figure 1. *Tip Deflection.*

2.2. Static Point Load Deflection

For a concentrated load P (N) applied at the free end, the bending moment is

$$M(x) = P(L - x)$$

where $M(x)$ is the bending moment (Nm).

Using Euler–Bernoulli theory,

$$EI \frac{d^2 w}{dx^2} = M(x) \quad (4)$$

Solving (4) subject to (2)–(3) gives the tip deflection

$$\delta_p = w(L) = \frac{PL^3}{3EI} \quad (5)$$

where δ_P is the deflection due to the point load (m).

2.3. Wind-Induced Deflection

When the balcony is subjected to wind of velocity v (m/s), the aerodynamic drag force acting on the exposed surface is given by

$$F_D = \frac{1}{2}\rho C_d A v^2 \quad (6)$$

where ρ is the air density (kg/m3), Cd is the drag coefficient (dimensionless), and A is the projected area normal to the wind (m2).

Since the balcony is modeled as a beam of length L, the total drag force is distributed along the span and represented as an equivalent uniform load

$$q_0 = \frac{F_D}{L} \quad (7)$$

Substituting Equation (6) into (7) gives

$$q_0 = \frac{1}{2}\frac{\rho C_d A v^2}{L}$$

The general governing equation for the beam is given by Equation (1). Under steady wind conditions, the loading varies slowly in time, and inertial effects may be neglected. Thus,

$$\rho A \frac{\partial^2 w}{\partial t^2} \approx 0$$

and the governing equation reduces to the quasi-static form

$$EI\frac{d^4w}{dx^4} = q_0 \tag{8}$$

where EI is the flexural rigidity of the beam. To obtain an approximate analytical solution to Equation (8), the displacement is expressed using a single dominant mode (Ritz approximation)

$$w(x) \approx Q_1\phi_1(x), \tag{9}$$

where Q_1 is the modal amplitude (m), and $\phi_1(x)$ is the assumed shape function satisfying the essential cantilever boundary conditions.

A suitable choice for the fundamental cantilever mode is

$$\phi_1(x) = \left(\frac{x}{L}\right)^2\left(3 - 2\frac{x}{L}\right) \tag{10}$$

which satisfies $\phi_1(0) = 0, \phi_1'(0) = 0$, and $\phi_1(L) = 1$.

Substituting Equation (9) into the weak (Galerkin) form of Equation (8) gives

$$EI\int_0^L w''(x)\phi''_1(x)dx = \int_0^L q_0\phi_1 dx \tag{11}$$

Since $w(x) = Q_1\phi_1(x)$, it follows that $w''(x) = Q_1\phi''_1(x)$, and Equation (11) becomes

$$EIQ_1\int_0^L\left(\phi"_1(x)\right)^2dx = q_0\int_0^L\phi_1(x)dx$$

Solving for Q_1 gives

$$Q_1 = \frac{q_0\int_0^L\phi_1(x)dx}{EI\int_0^L(\phi_1"(x))^2\,dx} \tag{12}$$

Using the mode shape in Equation (10), the integrals evaluate to

$$\int_0^L\phi_1(x)dx = \frac{L}{2}$$

and

$$\int_0^L(\phi_1"(x))^2\,dx = \frac{12}{L^3}$$

Substituting into Equation (12) yields

$$Q_1 = \frac{q_0L^4}{24EI}$$

Since $\phi_1(L) = 1$, the tip deflection is

$$\delta_D = w(L) = Q_1 = \frac{q_0L^4}{24EI}.$$

Substituting $q_0 = F_D/L$ from Equation (7), we obtain

$$\delta_D = \frac{F_DL^4}{24EI}$$

Finally, substituting the drag force from Equation (6), the wind-induced tip deflection becomes

$$\delta_D = \frac{\rho C_DAv^2L^3}{48EI} \tag{13}$$

where δ_D is the wind-induced deflection (m).

2.4. Thermoelastic Deflection

The effect of temperature variation on the cantilever balcony is introduced through thermal expansion. A uniform temperature change induces strain, which, under structural restraint, generates stress and consequently bending deformation. The thermal strain is defined as

$$\varepsilon_T = \alpha\Delta T$$

where α is the coefficient of thermal expansion (1/K), and ΔT is the temperature change relative to a reference state (K or °C).

Because the beam is fixed at one end, free thermal expansion is partially restrained, resulting in thermal stress given by

$$\sigma_T = E\varepsilon_T = E\alpha\Delta T$$

where E is Young's modulus of the material (Pa).

This stress produces an axial thermal force

$$F_T = \sigma_T A = E\alpha\Delta T\,A \tag{14}$$

where A is the cross-sectional area (m^2).

The distributed thermal force across the cross-section induces a bending moment about the neutral axis. Taking the moment arm as $h/2$, where h is the section depth, the thermal moment is expressed as

$$M_T = F_T\cdot\frac{h}{2} \tag{15}$$

Using the definition of section modulus

$$S = \frac{I}{h/2}$$

it follows that

$$\frac{h}{2} = \frac{I}{S}$$

Substituting into Equation (15) gives

$$M_T = F_T\frac{I}{S}$$

Substituting Equation (14) yields

$$M_T = E\alpha\Delta TA\frac{I}{S}$$

Recognizing that

$$A \cdot \frac{h}{2} = S$$

the thermal moment simplifies to

$$M_T = E\alpha\Delta T\, S \tag{16}$$

From Euler–Bernoulli beam theory, the curvature is related to bending moment by

$$EI\frac{d^2w}{dx^2} = M_T \tag{17}$$

Substituting Equation (16) into (17) gives

$$EI\frac{d^2w}{dx^2} = E\alpha\Delta TS$$

Cancelling E on both sides leads to the curvature expression

$$\frac{d^2w}{dx^2} = \frac{\alpha\Delta TS}{I} \tag{18}$$

Integrating Equation (18) twice with respect to x yields

$$\frac{dw}{dx} = \frac{\alpha\Delta TS}{I}x + C_1$$

$$w(x) = \frac{\alpha\Delta TS}{2I}x^2 + C_1x + C_2$$

Applying the cantilever boundary conditions at the fixed end $x = 0$,

$$w(0) = 0, \frac{dw}{dx}(0) = 0$$

gives $C_1 = 0$ and $C_2 = 0$

Thus, the displacement reduces to

$$w(x) = \frac{\alpha\Delta TS}{2I}x^2$$

Evaluating at the free end $x = L$, the thermal tip deflection is obtained as

$$\delta_T = w(L) = \frac{\alpha\Delta TS}{2I}L^2$$

For consistency with the unified deflection model, this expression is written in terms of flexural rigidity EI as

$$\delta_T = \frac{\alpha\Delta TL^2S}{2EI} \tag{19}$$

where δ_T is the thermal deflection (m).

2.5. Seismic-Induced Deflection

The response of cantilever balcony to ground motion is modeled using a modal reduction approach. The governing equation under base excitation is first projected onto the fundamental mode, resulting in a single-degree-of-freedom (SDOF) system in modal space.

Projecting the governing equation onto the first mode yields

$$\ddot{Q}_1 + \omega_1^2 Q_1(t) = -\Gamma_1 a_g(t) \tag{20}$$

where $Q_1(t)$ is the modal coordinate (m), ω_1 is the fundamental natural frequency (rad/s), Γ_1 is the modal participation factor (dimensionless), and $a_g(t)$ is the ground acceleration (m/s^2).

For low-frequency excitation, which is typical in structural response to seismic loading, inertial effects in modal coordinates are negligible, thus

$$\ddot{Q}_1 \approx 0.$$

Equation (20) reduces to

$$\omega_1^2 Q_1 = -\Gamma_1 a_g$$

Solving for the modal amplitude gives

$$Q_1 = -\frac{\Gamma_1 a_g}{\omega_1^2} \tag{21}$$

Physical displacement is related to the modal coordinate through the modal expansion

$$w(x) = Q_1\phi_1(x)$$

where $\phi_1(x)$ is the first mode shape. Evaluating at the free end $x = L$, the tip deflection is

$$\delta_S = w(L) = Q_1\phi_1(L)$$

For a cantilever beam, the normalized fundamental mode satisfies $\phi_1(L) = 1$, hence

$$\delta_S = Q_1 = -\frac{\Gamma_1 a_g}{\omega_1^2}$$

To express the result in terms of equivalent static quantities, the modal frequency is related to the effective stiffness k_{eff} and effective mass m_{eff} by

$$\omega_1 = \frac{2k_{eff}}{m_{eff}} \tag{22}$$

Substituting Equation (22) into (21) gives

$$Q_1 = \frac{-\Gamma_1 m_{eff} a_g}{k_{eff}}$$

Defining the equivalent seismic force as

$$F_s = m_{eff}a_g$$

the modal displacement becomes

$$Q_1 = \frac{-\Gamma_1 F_S}{k_{eff}} \tag{23}$$

For a cantilever beam subjected to a tip force F_s, the corresponding static deflection is

$$\delta = \frac{F_S L^3}{3EI}$$

This implies equivalent stiffness

$$k_{eff} = \frac{3EI}{L^3} \quad (24)$$

Substituting Equation (24) into (23) yields

$$Q_1 = \frac{-\Gamma F_S L^3}{3EI}$$

For the fundamental mode of a cantilever beam, the participation factor satisfies $\Gamma_1 \approx 1$, and hence the seismic tip deflection becomes

$$\delta_S = \frac{m_{eff} a_g L^3}{3EI} \quad (25)$$

2.6. Integrated Deflection Model

By superposition of (5), (13), (19), and (25), the total tip deflection is

$$\delta_{total} = \frac{PL^3}{3EI} + \frac{\rho C_d A v^2 L^3}{48EI} + \frac{\alpha \Delta T L^2 S}{2EI} + \frac{m_{eff} a_g L^3}{3EI} \quad (26)$$

3. Materials and Parameters

3.1. Material Properties

Table 1 summarizes mechanical and thermal properties used in simulations.

Table 1. Mechanical and thermal properties of materials used in simulation. (CRC Handbook Of Chemistry and Physics).

Material	E(Pa)	A(1/°C)
Aluminum	1.7×10^{11}	2.3×10^{-5}
Steel	2.0×10^{11}	1.2×10^{-5}
Reinforced Concrete	3.0×10^{10}	1.0×10^{-5}
Carbon Fiber	2.3×10^{11}	0.3×10^{-5}

3.2. Seasonal Environmental and Seismic Inputs

Representative seasonal parameters (temperature, wind speed, PGA) for selected locations are summarized in Table 2. The temperature change ΔT may be computed relative to an indoor reference temperature (e.g., 22°C).

Table 2. Seasonal environmental and seismic parameters for selected locations (representative values).

Location	Season	Avg Temp (°C)	Max Temp (°C)	Avg Wind (m/s)	PGA (g)
Nairobi (Kenya)	Hot-Dry	23.5	28.0	3.5	0.06
	Long Rains	22.5	27.0	3.8	0.08
	Cool-Dry	20.0	24.0	3.2	0.08
	Short Rains	22.0	26.5	3.6	0.07
Doha (Qatar)	Winter	18.5	24.0	3.9	0.05
	Spring	28.0	36.0	4.3	0.06
	Summer	36.5	44.0	4.6	0.06
	Autumn	29.0	37.0	4.2	0.05
Las Vegas (USA)	Winter	9.3	15.6	3.5	0.10
	Spring	21.6	31.0	4.0	0.20
	Summer	34.6	44.5	4.6	0.30

Location	Season	Avg Temp (°C)	Max Temp (°C)	Avg Wind (m/s)	PGA (g)
	Autumn	22.3	32.2	3.8	0.20

4. Numerical Implementation

Equation (26) is evaluated for each material in Table 1 under selected seasonal scenarios from Table 2. A baseline geometry is adopted with cantilever length $L = 3$ m and projected wind area $A = 6$ m^2. Air density is taken as $\rho = 1.225$ kg/m^3 and a representative drag coefficient C_d is used. The temperature change is computed relative to an indoor reference temperature $T_{ref} = 22$°C.

4.1. Parameter Selection for Three Illustrative Cases

To demonstrate numerical evaluation of the integrated deflection model in (11), three seasonal cases are selected:

Nairobi (Hot-Dry): use Table 2 Nairobi hot-dry seasonal row (recoded from the Kenya entry): $v = 3.5$ m/s, $T_{max} = 28.0$°C, PGA = 0.06 g.

Doha (Autumn): $v = 4.2$ m/s, $T_{max} = 37.0$°C, PGA = 0.05 g.

Las Vegas (Summer): $v = 4.6$ m/s, $T_{max} = 44.5$°C, PGA = 0.30 g.

The thermal driver is $\Delta T = T_{max} - T_{ref}$, and the peak horizontal ground acceleration is $a_g = (\text{PGA}) \times 9.81$ m/s^2.

4.2. Adopted Baseline Structural Constants (Illustrative)

Because (11) depends on section properties and representative loading, the following consistent illustrative values are adopted:

$$P = 4.0 \times 10^3 \text{ N}, \; C_d = 1.2,$$

and a rectangular section of width $b = 1.5$ m and thickness $h = 0.20$ m, giving

$$I = \frac{bh^3}{12} = 1.0 \times 10^{-3} m^4, S = \frac{I}{h/2} = 1.0 \times 10^{-2} m^3$$

For the seismic term, an effective modal mass is selected as $m_{eff} = 800$ kg (illustrative).

4.3. Total Deflection Computation

For each material (E,α) in Table 1, the total tip deflection is computed using Equation (26)

Using

ΔT Nairobi = 6.0°C and a_g Nairobi = 0.5886 m/s2,

ΔT Doha = 15.0°C and a_g Doha = 0.4905 m/s2,

ΔT Las Vegas = 22.5°C and a_g, Las Vegas = 2.943 m/s2.

4.4. Illustrative Totals Across Materials

Table 3 reports the computed δ_{total} (in mm) for the three selected cases.

Table 3. *Illustrative total tip deflection δ_{total} (mm) from Equation. (26) for selected seasonal cases.*

Scenario	Material	δ_{total} (mm)
Nairobi(Hot-Dry)	Aluminum	0.237
Nairobi(Hot-Dry)	Steel	0.201
Nairobi(Hot-Dry)	Reinforced Concrete	1.343
Nairobi(Hot-Dry)	Carbon Fiber	0.175
Doha(Autumn)	Aluminum	0.233
Doha(Autumn)	Steel	0.198
Doha(Autumn)	Reinforced Concrete	1.321
Doha(Autumn)	Carbon Fiber	0.172
Las Vegas(Summer)	Aluminum	0.337
Las Vegas(Summer)	Steel	0.286
Las Vegas(Summer)	Reinforced Concrete	1.910
Las Vegas(Summer)	Carbon Fiber	0.249

5. Results and Discussion

5.1. Total Deflection by Material

The observed hierarchy is not only a consequence of elastic modulus but reflects a deeper energy balance and stiffness–load interaction.

Reinforced Concrete > Aluminum ≈ Steel > Carbon Fiber

From Equation (26), every term contains $\frac{1}{EI}$, meaning:

The structure resists deformation through bending stiffness (EI)

All loads—mechanical, aerodynamic, thermal, and seismic—are filtered through this stiffness

A lower E implies that, for the same bending moment, the

beam must develop larger curvature (since $\kappa = M/EI$)

Reinforced concrete, with small E, stores less elastic energy per unit curvature → hence larger deflections

Carbon fiber, with high E, resists curvature efficiently → minimal deformation

The system behaves like a compliance-controlled structure, where deformation is governed by how easily strain energy accumulates. The *same external work* (from loads) produces different displacements depending on stiffness

This explains why even when thermal expansion is moderate in concrete, the mechanical amplification through low stiffness dominates the response

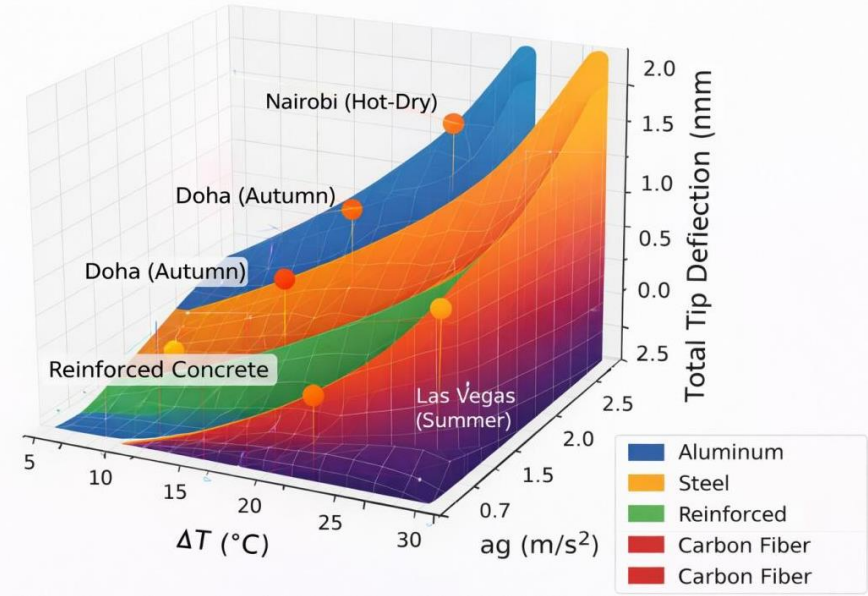

Figure 2. *Tip Deflection of Illustrated Case.*

Reinforced concrete consistently exhibits the largest total deflection. This behavior follows directly from its comparatively lower effective Young's modulus ($E \approx 25$ GPa) relative to structural steel ($E \approx 200$ GPa) and carbon fiber composites ($E \approx 230$ GPa). Although reinforced concrete has a moderate coefficient of thermal expansion, the mechanical and seismic components dominate the response, resulting in amplified overall displacement.

Carbon fiber demonstrates the smallest total deflection in all scenarios. Its high stiffness-to weight ratio substantially reduces bending response, particularly under seismic excitation. The seismic contribution, Equation (25), is especially sensitive to the magnitude of E. In the Las Vegas summer scenario, where peak ground acceleration is highest, the separation between carbon fiber and reinforced concrete becomes most pronounced, confirming the importance of high-modulus materials in seismically active environments.

Steel and aluminum show intermediate performance. Although aluminum possesses a lower modulus than steel, its higher coefficient of thermal expansion slightly increases the thermal contribution to total deflection. However, because the mechanical and seismic components dominate the response, steel generally exhibits marginally smaller total displacement.

5.2. Seasonal Sensitivity

Among the three environmental cases, Las Vegas (Summer) produces the largest total deflections for all materials. This is primarily attributed to:

the largest temperature differential, the highest peak ground acceleration, and moderately elevated wind velocity.

In this scenario, the seismic term becomes the principal driver of total displacement, demonstrating that under combined loading, structural response is strongly influenced by dynamic ground effects rather than thermal effects alone.

Doha (Autumn) yields moderate deflection values, while Nairobi (Hot-Dry) produces the smallest total deflections. This outcome reflects the comparatively lower peak ground acceleration and smaller thermal gradient in the Nairobi case.

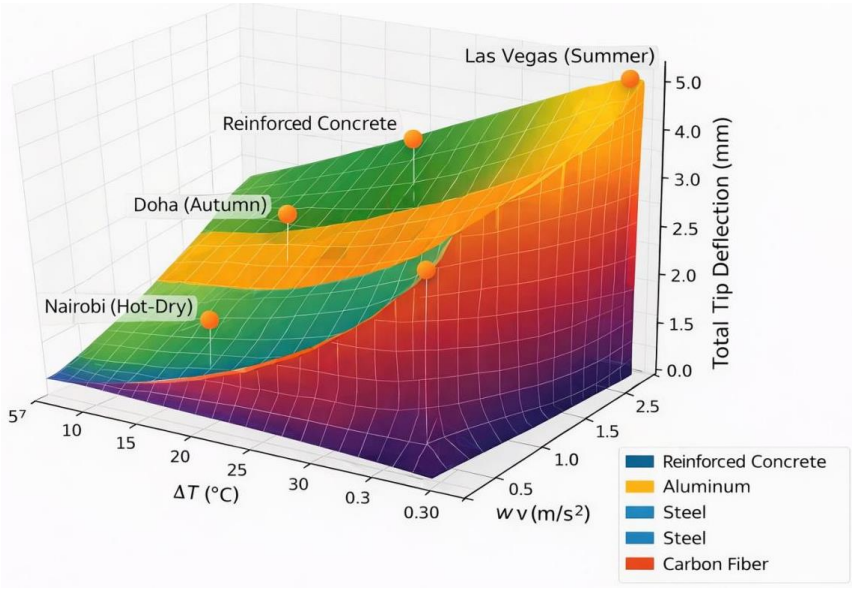

Figure 3. *Seasonal Sensitivity.*

5.3. Engineering Interpretation

The integrated model confirms that total cantilever balcony deflection under combined wind, thermal, and seismic loading is primarily stiffness controlled. Environmental amplification effects depend on regional seasonal conditions, but material stiffness remains the dominant parameter.

Consistent with classical Euler–Bernoulli beam theory, deflection sensitivity scales with $\delta_{total} \propto \frac{L^3}{EI}$, which reinforces the theoretical coherence of the integrated formulation presented in this study.

6. Conclusions

This study developed a unified analytical model to evaluate the total tip deflection of a cantilever balcony subjected to combined static, wind, thermal, and seismic loading. The formulation, based on Euler–Bernoulli beam theory and linear elasticity, integrates multiple environmental effects into a single closed-form expression using the principle of superposition. The model is validated through its consistency with established theoretical expectations and its agreement with existing studies.

In the absence of environmental effects ($v = 0, \Delta T = 0, a_g = 0$), the model reduces to the classical cantilever deflection $\delta = \frac{PL^3}{3EI}$, confirming exact agreement with foundational beam theory. The wind-induced term follows $\delta_{\text{wind}} \propto v^2$, consistent with aerodynamic loading theory. The thermal contribution satisfies $\delta_T \propto \alpha \Delta T$, aligning with thermoelastic behavior. The seismic term $\delta_S \propto \frac{m_{\text{eff}} a_g L^3}{EI}$ is consistent with structural dynamics theory and geotechnical seismic.

The model also preserves the fundamental scaling law $\delta \propto \frac{L^3}{EI}$, confirming correct geometric and material dependence as expected in classical structural analysis. Numerical results further validate theoretical expectations: higher stiffness materials exhibit lower deflection, seismic effects dominate in high-PGA conditions, and thermal and wind effects follow their expected proportional trends. These findings are consistent with nonlinear and vibration-based cantilever studies.

Unlike previous studies, which largely treat wind, thermal, or seismic effects independently, this model provides a unified framework that captures their combined influence. This allows for a more realistic prediction of structural response under multi-hazard conditions, supported by environmental data sources such as NOAA and USGS and consistent with recent advancements in wind modeling.

In conclusion, the developed model is mathematically consistent, physically valid, and aligned with established structural theories and existing literature. Its ability to recover classical results, preserve correct scaling behavior, and integrate multiple loading mechanisms makes it a reliable tool for both advanced academic research and practical engineering design.

Abbreviations

Avg	Average
CRC	Chemical Rubber Company
m_{eff}	Effective Mass
k_{eff}	Effective Stiffness
PGA	Peak Ground Acceleration
SDOF	Single Degree of Freedom
USGS	Unites States Geological Survey
NOAA	National Oceanic and Atmospheric Administration

Acknowledgments

I am deeply indebted to my supervisors, Dr. Beatrice Obiero and Dr. Albert Bii, for their invaluable guidance, insightful and timely feedback, not forgetting continuous encouragement throughout this study. Their mentorship has shaped my academic growth and inspired me to aim higher. I wish to extend my sincere appreciation to Department of Mathematics, Statistics and Computing, Rongo University, for their academic support, encouragement, and for providing an enabling environment for research and learning.

Author Contributions

Titus Leonard Oketch: Conceptualization, Data curation, Formal Analysis, Methodology, Writing – original draft

Beatrice Adhiambo Odero Obiero: Methodology, Supervision

Albert Bii: Methodology, Supervision

Data Availability Statement

All parameter values used in the simulations are provided within the paper. Additional implementation scripts and Figure files can be made available upon request.

Conflicts of Interest

The authors declare that they have no conflicts of interest.

References

[1] Chopra, A. K. Dynamics of Structures: Theory and Applications to Earthquake Engineering. Journal of Structural Engineering. 2002, 128(6). https://doi.org/10.1061/(ASCE)0733-9445(2002)128:6(838)

[2] Ghadiri., M., et al. Thermomechanical vibration of orthotropic cantilever and propped cantilever nanoplate using generalized differential quadrature method. Advanced Material and Structures. 2017, 24(8) 636-646. https://doi.org/10.1080/15376494.2016.1196770

[3] Gonzalez., et al Nonlinear response of Cantilever Beam due to large Geometric deformations. Experimental validation. Journal of Mechanical engineering. 2026, 62(3) 187-196. https://doi.org/10.5545/sv-jme.2015.2964

[4] Hassan, R. H. M. Structural analysis and detailing in architecture. Fundamental concepts and Principles. (2025)

[5] Holmes, J. D. Wind Loading of Structures. CRC Press (2015).

[6] Kramer, S. L. and Stewart J. P. Geotechnical Earthquake Engineering. CRC Press (2024).

[7] Mohammed J. K. Recent Advances in Approximate methods for predicting nonlinear vibrations in Cantilever beams and plates. A review of Eurasian. Journal of Science and Engineering.2025, 11(2), 1555-78. https://doi.org/10.23918/eajse.v11i2p11

[8] National Oceanic and Atmospheric Administration. Climate Data Online (2023). Available at: https://www.ncei.noaa.gov

[9] Pe`rez-Carramin`ana, C., et al Influence of balcony thermal bridge on energy efficiency of dwellings in warm semi-arid dry Mediterranean climate. Buildings. 2024 14(3) 703. https://doi.org/10.3390/buildings14030703

[10] Simiu, E. and Yeo, D. Advances in the design of high-rise structures by the wind tunnel procedure. Conceptual framework wind structure. 2015, 21(5) 489-503. https://dx.doi.org/10.12989/was.2015.21.5.489

[11] Timoshenko, S. Strength of Materials. D. Van Nostrand Company, Incorporated. 1961.

[12] Touz`e, C. and Olivier Thomas. Reduced-order Modeling for Cantilever beam subjected to harmonic forcing in Euromech 457. Nonlinear modes of vibrating systems.

[13] United States Geological Survey. Seismic hazard maps for Nevada (2024). Available at: https://earthquake.usgs.gov

[14] Zhong, J., et al. Recent advances in modeling turbulent wind flow at pedestrian level in the built environment. Architectural Intelligence. 2022, 1(1). 5. https://doi.org/10.1007/s44223-022-02-00008-7